Alfvén cascade eigenmodes above the TAE-frequency and localization of Alfvén modes in D–^{3}He plasmas on JET

Dreval, M.; Sharapov, S.E.; Kazakov, Ye. O.; Ongena, J.; Nocente, M.; Calado, R.; Coelho, R.; Ferreira, J.; Figueiredo, A.; Fitzgerald, M.

Total number of authors:
20

Published in:
Nuclear Fusion

Link to article, DOI:
10.1088/1741-4326/ac45a4

Publication date:
2022

Document Version
Early version, also known as pre-print

Alfvén cascade eigenmodes above the TAE-frequency and localization of Alfvén modes in D-^{3}He plasmas on JET

M. Dreval[1,2a)], S.E. Sharapov[3], Ye.O. Kazakov[4], J. Ongena[4], M. Nocente[5,6], R. Calado[7], R. Coelho[7], J. Ferreira[7], A. Figueiredo[7], M. Fitzgerald[3], J. Garcia[8], C. Giroud[3], N.C. Hawkes[3], V.G. Kiptily[3], F. Nabais[7], M.F.F. Nave[7], H. Weisen[9], T. Craciunescu[10], M. Salewski[11], Ž. Štancar[12] and JET Contributors[b)]

[1] *Institute of Plasma Physics, National Science Center, Kharkov Institute of Physics and Technology,61108 Kharkov, Ukraine*
[2] *V.N. Karazin Kharkiv National University, Kharkiv, Ukraine*
[3] *Culham Centre for Fusion Energy (CCFE), Culham Science Centre, Abingdon, UK*
[4] *Laboratory for Plasma Physics, LPP-ERM/KMS, TEC Partner, Brussels, Belgium*
[5] *Dipartimento di Fisica, Università di Milano-Bicocca, Milan, Italy*
[6] *Institute for Plasma Science and Technology, National Research Council, Milan, Italy*
[7] *Instituto de Plasmas e Fusão Nuclear, IST, Universdade de Lisboa, Lisboa, Portugal*
[8] *CEA, IRFM, Saint-Paul-lez-Durance, France*
[9] *Ecole Polytechnique Fédérale de Lausanne (EPFL), Swiss Plasma Center (SPC), Lausanne, Switzerland*
[10] *National Institute for Laser, Plasma and Radiation Physics, Bucharest, Romania*
[11] *Department of Physics, Technical University of Denmark, Kgs. Lyngby, Denmark*
[12] *Jožef Stefan Institute, Ljubljana, Slovenia*

[a)] Author to whom correspondence should be addressed: mdreval@kipt.kharkov.ua
[b)] See the author list of 'Overview of JET results for optimising ITER operation' by J. Mailloux et al to be published in Nuclear Fusion Special issue: Overview and Summary Papers from the 28th Fusion Energy Conference (Nice, France, 10-15 May 2021)

Abstract

Various types of Alfvén Eigenmodes (AEs) have been destabilized by fast ions over a broad frequency range from ~80 kHz to ~700 kHz in a series of JET experiments in mixed D-^{3}He plasmas heated with the three-ion ICRF scenario [M. Nocente et al., *Nucl. Fusion* **60**, 124006 (2020)]. In this paper, we identify the radial localization of AEs using an X-mode reflectometer, a multiline interferometer and soft X-ray diagnostics. The analysis is focused on the most representative example of these measurements in JET pulse #95691, where two different types of Alfvén cascade (AC) eigenmodes were observed. These modes originate from the presence of a local minimum of the safety factor $q_{\min}$. In addition to ACs with frequencies below the frequency of toroidal Alfvén eigenmodes (TAEs), ACs with frequencies above the TAE frequency were destabilized by energetic ions. Both low- ($f \approx$80-180 kHz) and high-frequency ($f \approx$ 330-450 kHz) ACs were localized in the central regions of the plasma. The characteristics of the high-frequency ACs are investigated in detail numerically using HELENA, CSCAS and MISHKA codes. The resonant conditions for the mode excitation are found to be determined by passing ions of rather high energy of several hundred keV and similar to those established in JT-60U with negative-ion-based NBI [M. Takechi et al., *Phys. Plasmas* **12**, 082509 (2005)]. The computed radial mode structure is found to be consistent with the experimental measurements. In contrast to low-frequency ACs observed most often, the frequency of the high-frequency ACs decreases with time as the value of q_{min} decreases. This feature is in a qualitative agreement with the analytical model of the high-frequency ACs in [B.N. Breizman et al., *Phys. Plasmas* **10** 3649 (2003)]. The high-frequency AC could be highly relevant for future ITER and fusion reactor plasmas dominated by ~ MeV energetic ions, including a significant population of passing fast ions.

1. Introduction

The three-ion D-(D_{NBI})-^{3}He ion cyclotron radio frequency (ICRF) scheme was recently successfully applied for plasma heating and fast-ion-physics studies in mixed D-^{3}He plasmas at JET [1-4]. In this series of experiments, co-passing fast deuterons from Neutral Beam Injection (NBI) with $E_{NBI} \approx 100$ keV were accelerated to energies up to ~2 MeV in the plasma center, following the core localization of the ion-ion hybrid (IIH) layer. The RF-accelerated D-NBI ions, in turn, produced alpha particles ($E_\alpha \approx 3.7$ MeV) via D-^{3}He fusion reactions. The fast-ion distribution of energetic deuterons was controlled by varying the ICRF and NBI power ($P_{ICRF} \approx$ 4-6 MW, $P_{NBI} \approx$ 3-20 MW), resulting in rather high D-D neutron ($\approx 1\times10^{16}$ s^{-1}) and D-^{3}He alpha rates ($\approx 2\times10^{16}$ s^{-1}) at moderate input heating power. An important difference between the three-ion ICRF heating of beam ions and more commonly used ICRF scenarios is that a significant population of MeV-range co-passing fast ions is generated with the three-ion scheme, as follows from theoretical results in [2, 3] and confirmed by TRANSP analysis [5].

A large variety of Alfvén Eigenmodes (AEs) in the frequency range varying from ~80 kHz to ~700 kHz were regularly destabilized by fast ions in these JET experiments [2-4]. The observed modes include the toroidicity-induced AEs (TAEs), ellipticity-induced AEs (EAEs), as well as reversed-shear AEs (RSAEs), referred to as Alfvén Cascades (ACs) [6] throughout this paper. Both ICRF-generated energetic deuterons and fusion-born alpha particles [4, 7] can resonate and excite AEs in contrast to the sub-Alfvénic NBI ions causing damping of AEs on JET. Studying the characteristics of AEs in these JET plasmas with strong core electron heating from MeV-range fast ions is also relevant for ITER and future fusion reactors, where similar conditions will be reached with alpha particles.

Figure 1 shows an overview of JET pulse #95691 heated with the three-ion D-(D_{NBI})-^{3}He scheme with $P_{NBI} \approx 6.7$ MW and $P_{ICRF} \approx$ 3.4-5.4 MW. This pulse is selected for our analysis as one of the most representative examples due to the simultaneous presence of AEs with very different frequencies. AEs were observed in all three-ion D-(D_{NBI})-^{3}He JET discharges but the chosen discharge has especially broad range of AE frequencies excited (see Fig. 3(a)). A substantial modification of the AE spectrum was identified during these experiments due to the changes in the plasma equilibrium. In particular, the observation of ACs implies the reversed-shear equilibrium as the presence of a local minimum of the safety factor, q_{min} is one of the necessary conditions for these modes to be destabilized [6].

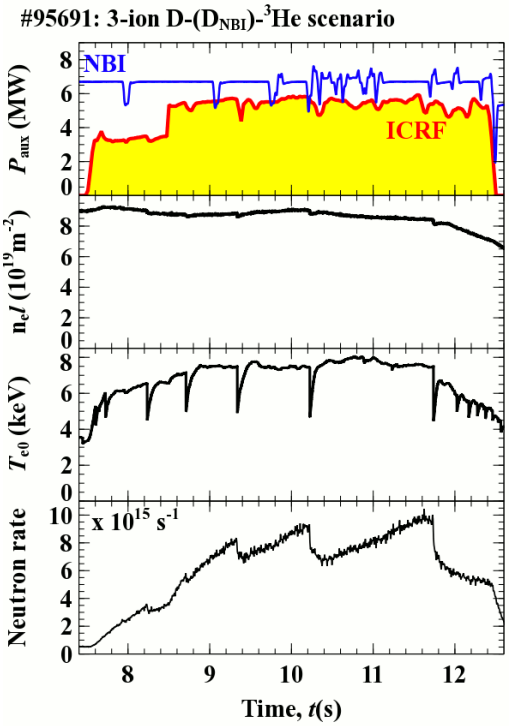

Figure 1. Overview of JET pulse #95691 (B_0 = 3.7T, I_p = 2.5MA), where a large variety of AEs were destabilized by energetic ions generated by the three-ion D-(D_{NBI})-^{3}He ICRF scenario in D-^{3}He plasma. The panels from top to bottom show NBI and ICRF power, the line-integrated central density, the central electron temperature and the D-D neutron rate.

Two different types of ACs were regularly observed during the long-period sawtooth phases in this series of JET experiments. In addition to low-frequency ACs with frequencies below the TAE frequency, also ACs with frequencies above the TAE frequency were destabilized by energetic ions. These modes are referred to as the high-frequency ACs (HFACs) throughout the paper [8]. Opposite to the characteristics of the low-frequency ACs, high-frequency ACs feature the temporal decrease of their frequency as the value of $q_{\min}$ decreases. HFACs were previously observed in reversed-shear plasmas in JT-60U experiments heated with negative-ion-based NBI, injecting a large number of passing ions with energies ~400 keV [9]. However, these modes were rarely observed on JET to be diagnosed sufficiently well, and the present paper fills in the gap in such mode measurements. The analysis reported in this paper highlights the similarity of the novel HFAC observations at JET to earlier JT-60U results, and reports on the presence of high-energy passing ions as one of the necessary conditions for these modes to be destabilized. As shown below, both low- and high-frequency ACs in these JET experiments were localized in the central regions of the plasma, as inferred from a range of JET diagnostics and supported by numerical modeling of the mode structure using MHD codes HELENA [10], CSCAS [11] and MISHKA [12]. The existence criteria and features of HFACs were analyzed analytically in [8]. Yet a consistent experiment-to-theory comparison of HFACs is lacking and this is a main subject of this work. These modes could also be highly relevant for future ITER plasmas dominated by fusion-born alpha particles, including a large population of MeV-range passing ions.

The HFAC modes are localized in vicinity of the local minimum of the safety factor profile q_{min} and exist due to the non-monotonic safety factor profile similar to the usual AC with frequency below TAE. However, as shown in Ref. [8], the frequency of HFACs decreases with $q_{\min}$ decreasing, in contrast to AC's with frequencies below the TAE-frequency. A basic

understanding of the AC and HFAC nature can be obtained from a simple approach. The AC frequency can be estimated using the formula

$$\omega = \frac{V_A}{R_0}\left| n - \frac{m}{q_{\min}} \right|, \qquad (1)$$

where m, n are poloidal and toroidal mode numbers, V_A is the Alfvén velocity, R_0 is the major radius. In Eq. (1), the $n\text{-}m/q_{min}$ factor originates from the parallel wavevector $k_{||}$ and is a strong function of q_{min}, as it is combined with m values, which are usually higher than unity. Thus, the major contribution to the evolution of AC frequency is introduced by the temporal evolution of q_{min} value, and a weaker contribution comes from temporal variations in V_A. Considering now the TAE-gap frequency, $\omega_{\mathrm{TAE}}=V_A/(2qR_0)$, we note that $n\text{-}m/q_{min}$ can be either lower than $1/(2q)$ for the usual AC with frequencies below TAE, or $n\text{-}m/q_{min}$ can be higher than $1/(2q)$. It is the latter case that corresponds to HFACs consequently. The AC frequency evolution from the zero frequency (actually, from minimal frequency depending on the Geodesic Acoustic Mode (GAM) frequency f_{GAM} [13] and the frequency due to the temperature gradient f_∇ if applying a more accurate description [14]) up to the TAE frequency follows from this approach. The more accurate formula for the low frequency AC is given by

$$f = \sqrt{f_1^2 + f_{GAM}^2 + f_\nabla^2}\ , \qquad (2)$$

where $f_1 = \omega/(2\pi)$ is a frequency from Eq. (1). In contrast, the HFAC frequency is bounded between the TAE frequency and the EAE frequency of $\omega_{\mathrm{EAE}}=V_A/(qR_0)$, well above the GAM frequency. Both TAE and EAE gap boundaries are seen from the evolution of the HFAC frequency as q_{min} decreases. In this approach, increase or decrease of the q_{min} value causes increase or decrease of the AC frequency, but only certain frequencies given by Equations (1) and (2) are suitable for establishing an eigenmode [8]. The HFAC can be observed simultaneously with the usual AC. The HFAC modes were frequently observed in the three-ion ICRF discharges in JET, and this makes it possible to investigate HFAC modes numerically by MHD spectral codes in this work. Such experimental data as radial location and toroidal mode numbers of the HFAC are compared with results of the numerical modeling in our work.

2. Experimental setup

The experiments were undertaken at a central toroidal magnetic field $B_0 = 3.7$ T, plasma current $I_p = 2.5$ MA, central electron densities $n_{e0} \approx 6\times10^{19}$ m^{-3}, ICRF frequency $f = 32.2$-33.0 MHz (dipole antenna phasing) such that the cyclotron resonances for thermal D and ^{3}He-ions were located off-axis at the high- and low-magnetic field side, respectively. Rather large ^{3}He concentrations, $n(^3\mathrm{He})/n_e \approx 20$-$25\%$, were purposely chosen to position the ion-ion hybrid layer in the plasma core, such that energetic deuterons from NBI are accelerated in the plasma centre [1-4]. The toroidal array of Mirnov coils has been used to determine the toroidal mode numbers of the destabilized modes. Furthermore, a range of internal diagnostics is available on JET that allows to identify the radial mode localization. The multi-chord interferometer is one of such diagnostics. The central interferometer has a vertical line-of-sight passing through the plasma center (see the blue line in Figure 2) and is useful to monitor modes in the central regions of the plasma.

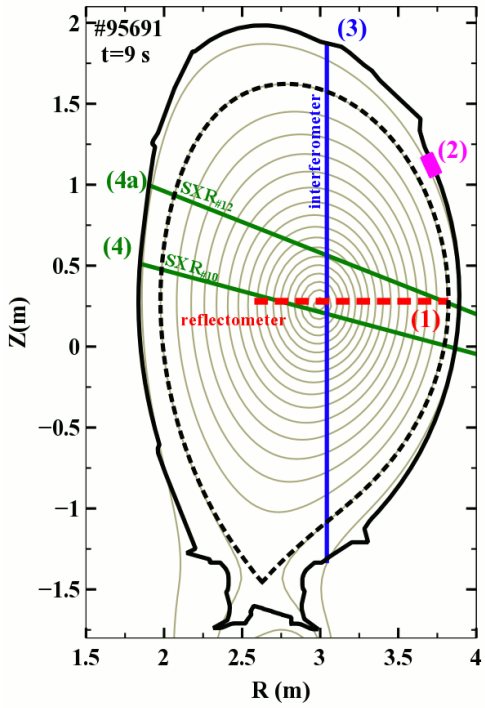

Figure 2. The lines-of-sight and position of different diagnostics used to characterize AEs in JET pulse #95691. (1): the correlation reflectometer; (2) Mirnov magnetic coil; (3) central interferometer; (4) SXR channel #10; (4a) SXR channel #12.

In this work, we also use the channel #10 of the soft X-ray (SXR) diagnostics (cf. green line in Figure 2) for monitoring the modes in the plasma core. The set of SXR lines of sight can be potentially used for a more accurate mode localization. However, the low spatial resolution in central region due to high angular step between neighboring SXR channels and the existing SXR hardware restrictions in sensitivity and frequency resolution limit this possibility in JET. The main tool in our work is the microwave reflectometer. In contrast to the SXR or interferometer diagnostics, the X-mode reflectometer provides local measurements of density fluctuations in the plasma core. We use the F-band X-mode correlation reflectometer [15] with a pre-programmed frequency sweep [16] for the mode localization assessment. The frequency sweep used in the reflectometer simplifies AE modes localization in contrast to the set of fixed during discharge frequencies. Diagnostic principles of reflectometric density fluctuation measurement and AE localization in JET are described in Ref. [15]. We are describing only selected points relevant to our results here. Only one channel of the correlation reflectometer is used because the pre-programmed frequency separation between two channels was optimized for turbulence measurements and was insufficient for resolving spatial structure of AE modes. The two channels show identical results consequently.

A location of the reflectometer measurement is determined by location of the microwave cut-off layer. The X-mode microwave cut-off position is determined by the cut-off frequency. The X-mode microwave cut-off frequency f_R described as following formula: $f_R = 0.5 f_c + \sqrt{0.25 f_c^2 + f_p^2}$, where f_{ce} is electron cyclotron frequency and f_{pe} is plasma frequency. Thus, the two main parameters, namely the magnetic field (via f_{ce}) and the plasma density (via f_{pe}), determine the cutoff position. The EFIT equilibria [17] restricted with the Motional Stark Effect (MSE) diagnostic [18] are used in our work for the evaluation of the magnetic field profile. Note that the accuracy of the radial cutoff localization is higher at the low magnetic field side, where both the magnetic field and the plasma density increase toward the

magnetic axis. Two different diagnostics for the plasma density profile are used to assess an uncertainty of the cutoff position: the *X*-mode cutoff radial position inferred on the basis of the density profiles given by the KG10 reflectometer [19] and the LIDAR Thomson scattering [20, 21] diagnostics are displayed as solid black and dashed green lines in Figures 6(d) and 8(b), respectively.

3. Experimental results.

3.1. Overview

Figure 3(a) shows the spectrogram of the Mirnov coil signal in JET pulse #95691 ($P_{ICRF} \approx 5.4$ MW, $P_{NBI} \approx 6.7$ MW). In this pulse, various types of AEs were destabilized by fast ions, including TAEs, tornado TAEs [22], EAEs and two different types of ACs. The correlation between AEs and sawtooth oscillations can be obtained from Figures 3(a) and (b). Figures 3(c) and (d) show the inferred toroidal mode numbers of the high frequency ACs [8, 9] and the usual ACs between two monster sawtooth crashes at $t = 9.34$s and $t = 10.23$ s. As follows from Figure 3(c), the high-frequency AC with n=2 was observed starting from $t = 9.7$ s. Interestingly, a set of short-lived modes with $n = -1$, $n = 0$ and $n = +1$ in the frequency range of HFACs was also observed during $t \approx 9.43$-9.48 s. These modes appear shortly after the monster sawtooth crash, which substantially modifies the fast-ion distributions and the q-profile [2-4], and are outside the scope of the present paper. Note that the usual ACs were not observed during that stage.

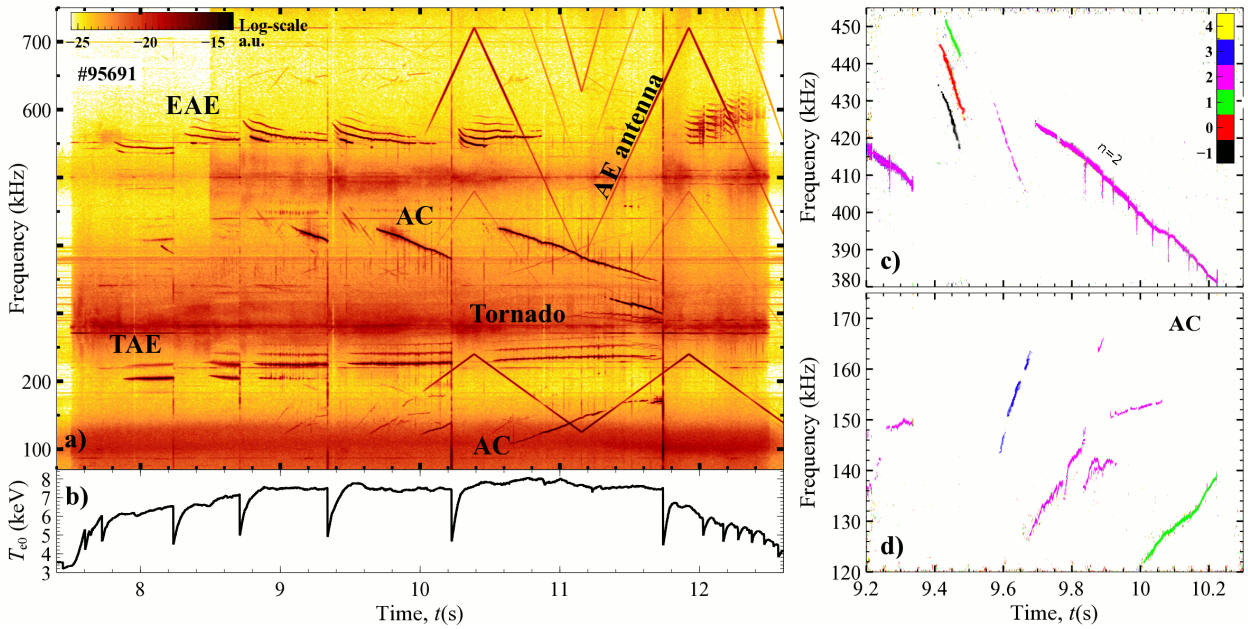

Figure 3. (a) The spectrogram of the Mirnov coil signal in JET pulse #95691 heated with the three-ion D-(D_{NBI})-^{3}He ICRF scenario. . (b) The temporal evolution of the central electron temperature. (c) and (d) The toroidal mode numbers of the high-frequency and low-frequency Alfvén cascades ($t = 9.2$-10.3 s).

The characteristics of AC and HFAC modes are strongly sensitive to the details of the safety factor profile q. Figure 4 shows the q-profile in JET pulse #95691 at $t = 9.8$ s, inferred from the MSE diagnostic [18]. The error bars in the q-profile measurements are marked by the shadow area in Fig. 4.

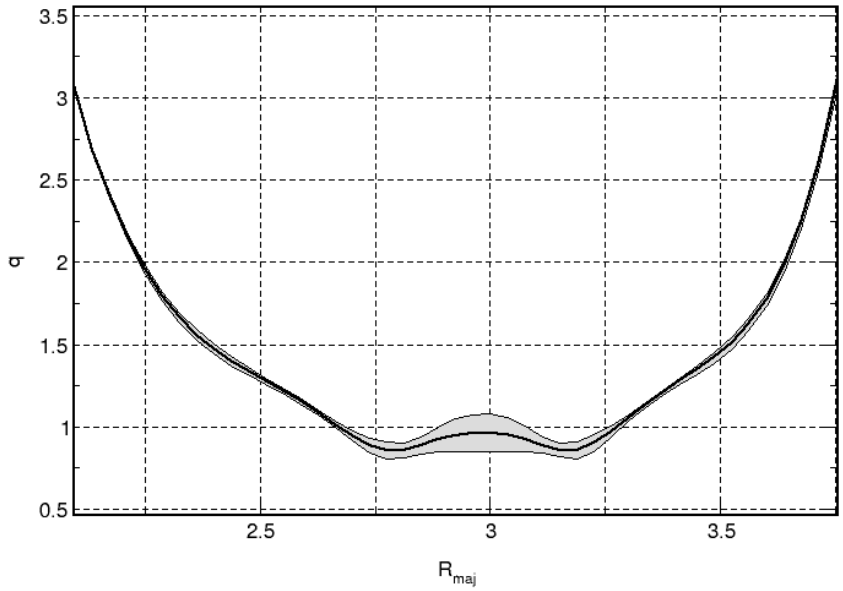

Figure 4. The radial dependence of the q-profile together with the estimated errorbars in JET pulse #95691 at t = 9.8 s, as inferred by the MSE diagnostic.

Soft X-ray (SXR) and interferometer diagnostics are used for estimation of radial location of the modes. Spectrograms of the central interferometer channel data and central SXR channel data are shown in Figure 5, confirming the destabilization of the conventional and high-frequency Alfvén cascades, TAEs and tornado TAEs ($f \approx 300$ kHz) in JET pulse #95691. Despite the line-integrated nature of the interferometer and SXR signals, a contribution of the edge fluctuations to the central lines-of-sights is usually not significant. The AC and high-frequency AC are seen by the central lines-of-sights only. Thus these observations indicate that the observed modes are localized in plasma core region.

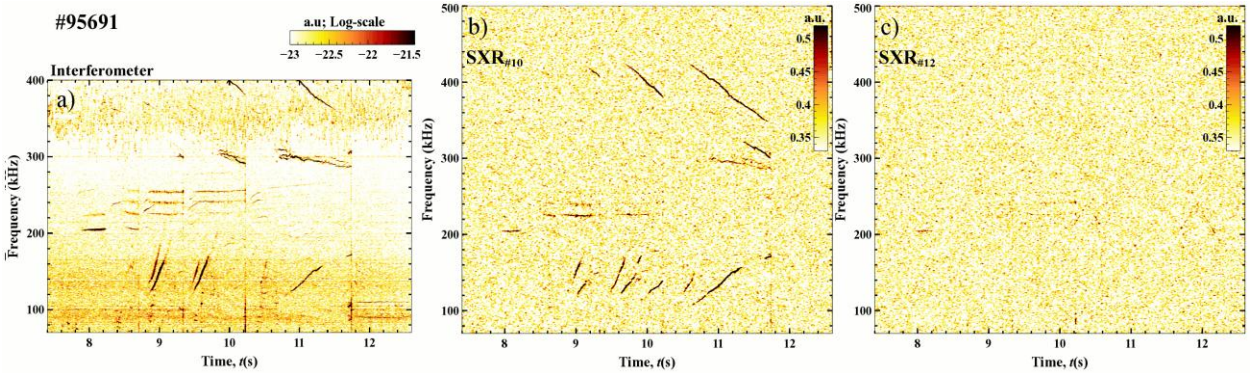

Figure 5. a) The spectrogram of the central interferometer. . (b) and (c) The cross-correlation of the Mirnov coil with SXR #10 and SXR #12 signals in JET pulse #95691.

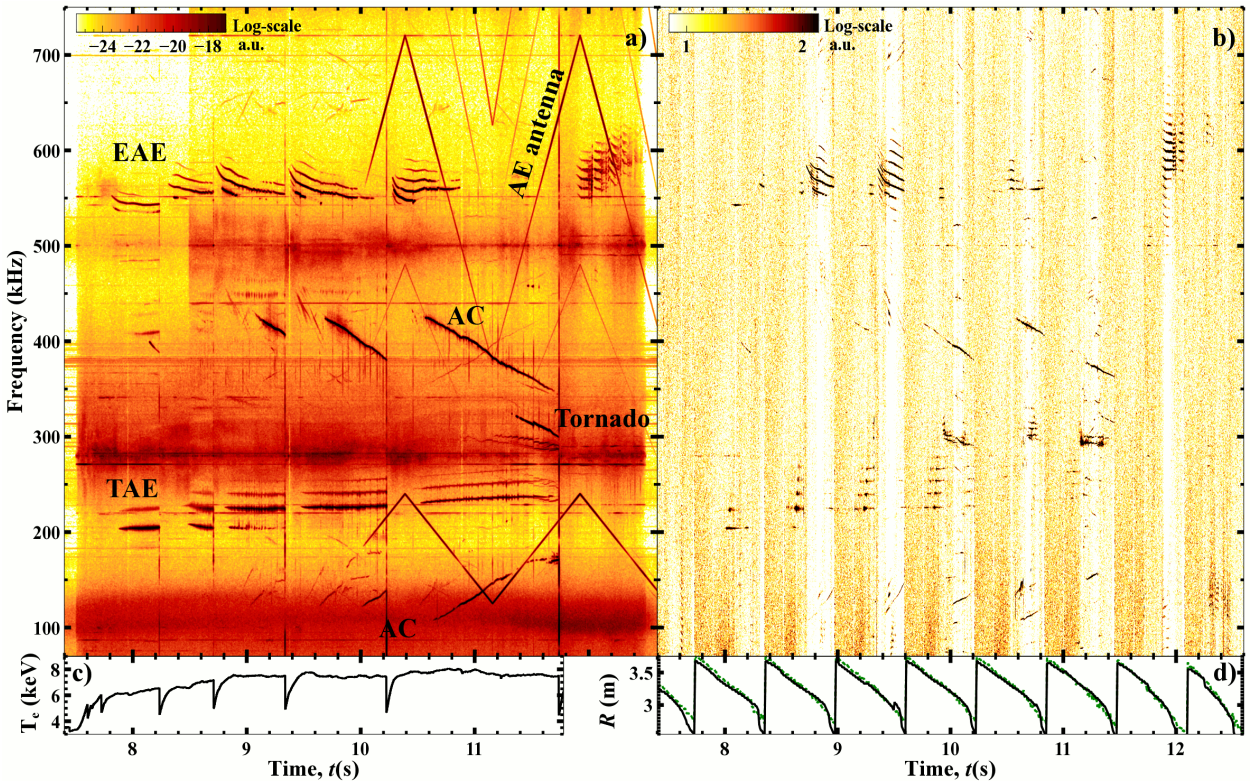

Figure 6. a) spectrogram of Mirnov coil signal; c) waveform of central electron temperature b) spectrogram of reflectometer signal; d) radial location of the reflectometer cut-off position.

Further information on the radial localization of these modes can be inferred by comparison of two panels shown in Fig. 6. The Mirnov coil spectrogram (Fig. 6(a)), measured at a fixed spatial location, shows the temporal evolution of the modes and their dependencies on the variation of plasma parameters, in particular, the sawtooth oscillations (Fig. 6(c)). In contrast, the spectrogram of the correlation reflectometer signal (Fig. 6(b)) contains a mixed information on the temporal evolution of modes and their radial dependencies. Indeed, the radial measurement point of the reflectometer is periodically moved through the plasma, following the preprogrammed sweeps of the frequency of the probing microwave. The major radius of the *X*-mode cutoff in JET pulse #95691 is shown in Fig. 6(d). As follows from Fig. 6, both low- and high-frequency ACs are localized in the central region of the plasma $R \approx 2.8$-3.2 m. A more detailed analysis of HFACs is given in the next sub-section of the paper.

3.2. MHD analysis of HFACs

More quantitative analysis of HFACs, including the calculation of AE gaps in the Alfvénic continuum and the mode radial structure, was carried out using a set of MHD codes HELENA [10], CSCAS [11] and MISHKA [12]. The largest uncertainties in these calculations are mainly determined by uncertainties in the safety factor, in particular, in the plasma core. In this paper, we consider four different q-profiles shown in Fig. 7(a): i) a monotonic q-profile with $q_0 = 0.96$ (black line); ii) a model inverted q-profile with $q_0 = 0.96$ and $q_{\min} = 0.96$ (red line); iii) a model inverted q-profile with $q_0 = 0.84$ and $q_{\min} = 0.79$ (magenta line) and iv) the q-profile at $t = 9.9$ s inferred from MSE measurements (dashed green line). The radial coordinate s used in Fig. 7(a) is the square root of the normalized poloidal flux, i.e. $s = \psi_N^{1/2}$.

The model q-profiles in the central region of the plasma were constructed by the MHD-spectroscopy approach and the use of MHD markers [23]. As discussed in [24], TAEs and EAEs are localized at the radial locations, where:

$$q = \frac{2m + \mu}{2n}. \qquad (3)$$

Here, m and n are poloidal and toroidal mode numbers; μ=1 for TAE and μ=2 for EAE modes. The central EAEs are evidently linked with q=1 rational surface, for example for n=3 mode: $q = (m+1)/n = (2+1)/3 = 1$. Thus, we can localize the q=1 surface from the measured EAE location. Locations of the central n=3 and n=4 branches of TAEs observed at $q = (m+0.5)/n$, corresponding to q=1.16(6) and q=1.125 values. These values allow as to localize these two points at the $q(R)$ profile [8]. The presence of AC modes indicates that q-profile is not monotonic, since AC existence is caused by a local minimum of q [6]. A radial location of the minimum of the safety factor profile should coincide with the radial location of AC modes. Modeling radial profiles of the safety factor in the core region, reconstructed by abovementioned constraints are shown in figure 7(a). The q_1 profile corresponds to the stage of the discharges shortly after the Sawtooth crash. This profile is constructed by radial location of q=1 and q=1.16 values and by the EFIT q-profile at the plasma edge. The radial location of q=1 at $s \equiv \sqrt{\psi_N} \approx 0.25 - 0.3$ is estimated by Sawtooth inversion radius as well as is measured by the reflectometer EAE radial location, where ψ_N is normalized poloidal flux. The radial location of q=1.16 at $s \approx 0.45$ is estimated by radial location of n=3 TAE mode (see figure 6).

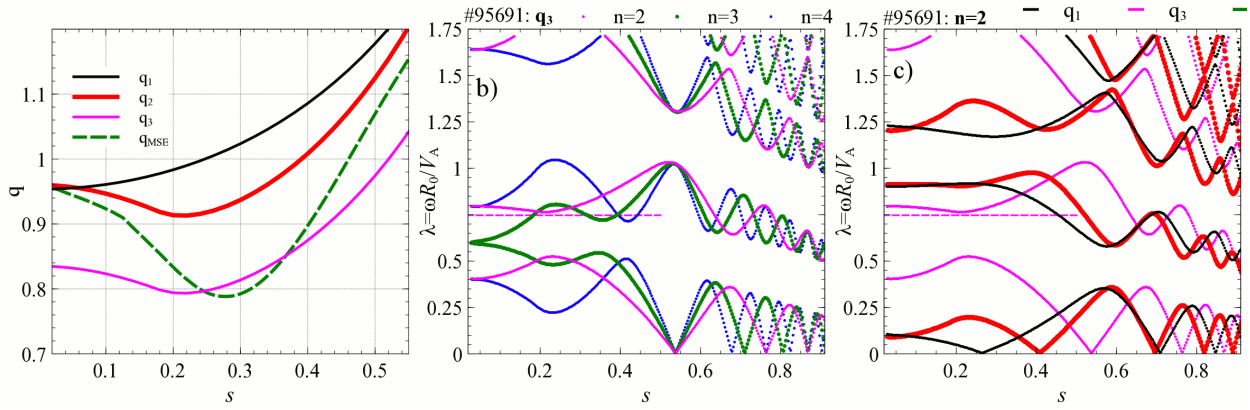

Figure 7. a) A set of the q-profiles used for MHD analysis of HFACs in JET pulse #95691. The dashed green line illustrates the inverted q-profile at $t = 9.9$ s, as inferred from MSE measurements. (b) The Alfvén continuum structures for toroidal mode numbers n=2-4, using q_3 as input. q_3. (c) The Alfvén continuum structures for q_1, q_2 and q_3 computed for $n = 2$. The horizontal dashed line marks the frequency and the radial localization of the $n = 2$ HFAC.

Synthetic modeling profiles q_2 and q_3 are developed for the AC calculations. The HFAC and usual AC are localized in the same region, as it is seen from the figure 6. This location corresponds to the q_{min} location of about $s \approx 0.2$-0.3 ($R \approx 3.2$m) as it is seen from figures 6,8. The value of q_{min} is deduced from the measured AC mode frequency via our numerical modeling. These radial location and value of q_{min} are the only constraints available. Under this constrains we can compute accurately the temporal evolution of the q_{min} (t) during HFAC evolution, but we cannot calculate the exact shape of the q profile. A parallel shift of the q_3 profile form q_2 without its shape distortion is used for simplicity of our calculations only. These profiles are used for demonstration of major HFAC features: radial location of HFAC center, poloidal mode number

and frequency. The q_2 profile corresponds to the stage of post-crash of Sawtooth plasma evolution, when both the AC and HFAC appear (See figure 3). The Alfvén continuum structures calculated by CSCAS code for q_2 profile and n=2-4 toroidal mode numbers are shown in figure 7(b). The q_{min} causes a formation of additional "hill" and "valley" of the continuum. The usual ACs are localized above the "hill" in the continuum [25]. The n=2 location and normalized frequency λ are calculated by the MISHKA code. It is marked by the dashed line in figure 7(b). Thus, the HFACs are localized below the "valley" of the continuum. This "valley" is clearly seen for the n=2 case. The continuum for the n=3,4 cases, forms a hill at q_{min} point. This hill-type extremum prevents HFAC formation according to the eigenmodes calculation. Therefore, due to this structure of the continuum, at the zero shear point of the q_{min} region, the n=3, 4 HFACs are not observed experimentally. The "valley" structure is observed in a family of q profiles in the case of n=2. This family is limited by q_2 and q_3 profiles. The required stability conditions are satisfied for the n=2 case only, according to our modeling. A comparison of the n=2 Alfvén continuum structures for q_2 and q_3 profiles is shown in figure 7(c). As it is seen from the figure, decrease of the q_{min} value causes the "valley" level decreasing and decreasing of the HFAC mode frequency consequently. This dependence of the frequency of the high frequency AC on the q_{min} value agrees with analytical description [8] and experimental observations. The observed increase of the usual AC frequency and the decrease of the HFAC frequency (see figure 3**)** are linked with the decrease of q_{min}. The zoomed spectrogram of the reflectometer is shown in figure 8.

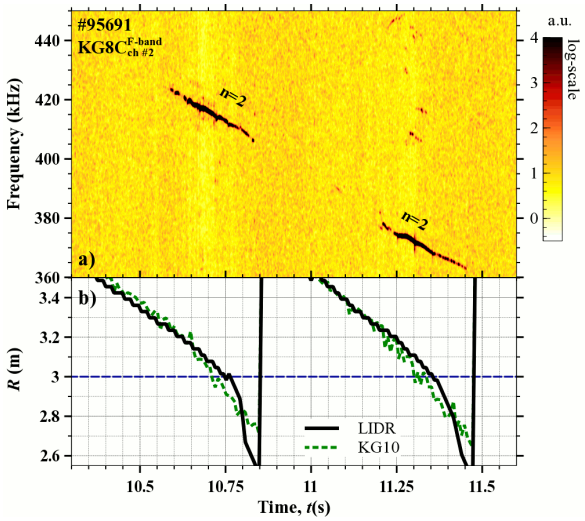

Figure 8. Localization of high frequency AC modes by reflectometer: a) spectrogram; b) location of cut-off by LIDAR (black) and KG10 (green).

The n=2 HFAC is localized at $R \approx$ 3.2-2.8m (at $s \approx 0.3$) at observed frequencies of =425-350 kHz (as seen from figures 3,6,8). The measured frequency consist of the mode frequency in the Lab reference frame f_{mode} and the Doppler effect due to toroidal plasma rotation $f=f_{\text{mode}}+n\,f_{\text{rot}}$. The frequency shift caused by the plasma rotation $f_{\text{rot}} \approx 10$ kHz is estimated from the EAE frequency separation, see figure 6. The EAEs are located at the q=1 surface, close to the AC and HFAC locations. Thus we can assume that the difference of the plasma rotations in these two locations is negligible. These frequencies correspond to normalized frequency of $\lambda = \omega R_0 / \upsilon_{A0} \approx 0.89\text{-}0.74$. Theses normalized frequencies are demonstrated by CSCAS and MISHKA calculations on the base of family of safety factor profiles like q_2 and q_3 in figure 7. Computed by MISHKA eigenmodes of HFAC for q_3 case are shown in figure 9. The wave potential ϕ and poloidal velocity V_θ presented in this figure are estimated from the MISHKA output parameters as $\phi \sim sV_r/m$ and $V_\theta \sim (1/m)\partial(sV_r)/\partial r$.

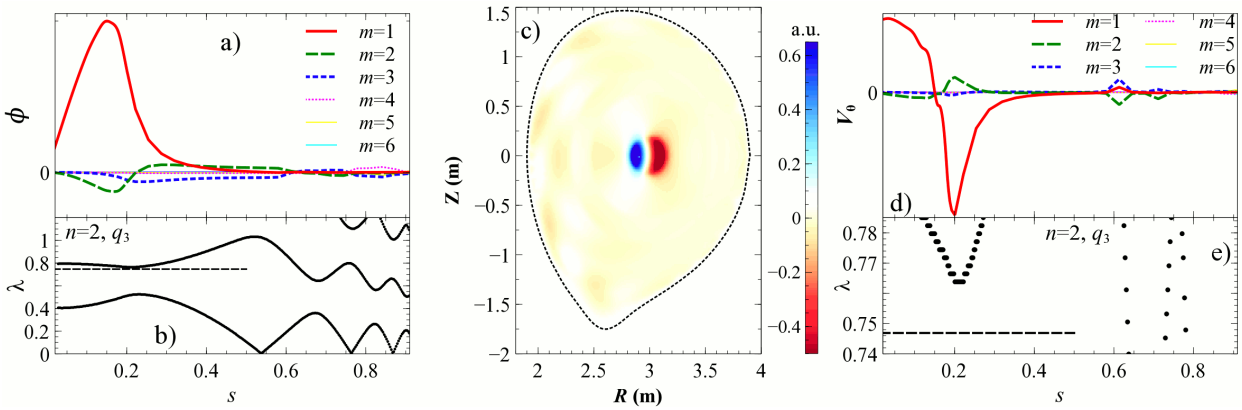

Figure 9. MISHKA calculation of HFAC modes, of plasma potential ϕ (a) and poloidal velocity V_θ (d); poloidal structure of ϕ and Alfvén continuum structures (b),(e). n=2 and q_3 profiles are used. We use a.u., only positive/negative sign makes sense.

The harmonics of V_θ peak is located at s≈0.2. Therefore, the wave energy ~ $(\partial\phi/\partial r)^2$ peaks at s≈0.2, coincides with the position of the minimum of the upper continuum branch. However, the computed mode structure is rather extended in radius and therefore can interact with energetic particles in an area from s=0 to s~0.4.

The EFIT equilibrium with the Motional Stark Effect diagnostics is used for validation of our results then. The safety factor profile q_{MSE} is obtained from this equilibrium at the stage of discharge corresponding to the q_3 modeling profile. The $q_{\min}$ values of these two profiles are equal, in spite of different shape. Computed by MISHKA eigenmodes of HFAC for q_{MSE} case are shown in figure 10. The poloidal mode numbers, radial locations of the mode center and normalized frequencies are almost equal in q_3 and q_{MSE} cases, as seen from figures 9 and 10. These results demonstrate additional confirmation of our MHD-spectroscopy-based modelling.

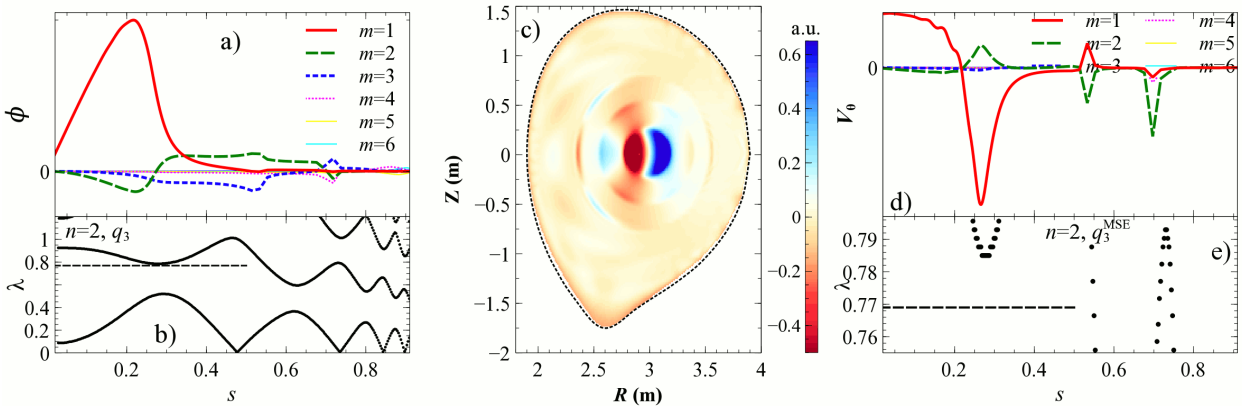

Figure 10. MISHKA calculation of HFAC modes, of plasma potential ϕ (a) and poloidal velocity V_θ (d); poloidal structure of ϕ and Alfvén continuum structures (b),(e). n=2 and q_{MSE} profiles are used. We use a.u., only positive/negative sign makes sense.

The observed characteristics of the n = 2 HFAC in JET pulse #95691 during the sawtooth cycles t = 9.34-10.23 s and t = 10.23-11.74 s are summarized in Table 1. The chosen time slices t = 9.7 s and t = 10.6 s correspond to the time, when the n = 2 HFAC was observed after the preceding monster sawtooth crash. The $q_{\min}$ values shown in Table 1 are calculated on the base of Eqs. (1) and (2), using the plasma rotation frequency of f_{rot}=10 kHz and the GAM frequency of 55 kHz. In these JET experiments, the influence of the temperature gradient term, f_∇ on the

HFAC eigenmode frequency [14] is less than ~3 kHz and can be ignored. At $t = 9.7$ s, we additionally evaluated $q_{\min} \approx 0.91$ using the characteristics of the observed $n = 2$ low-frequency Alfvén cascade ($f = 130$ kHz, $\lambda \approx 0.17$). This value is in a very good agreement with $q_{\min} \approx 0.89$ evaluated from the HFAC analysis at $t = 9.7$ s. Note that for the other time slices shown in Table 1 the $n = 2$ low-frequency AC was not observed (instead, the $n = 1$ AC was destabilized). The $q_{\min}$ values inferred from the analysis of ACs are consistent with experimental observations. Thus, this example shows another possible application of the MHD spectroscopy approach in reversed-shear equilibrium plasmas with destabilized ACs.

Table 1. Summary of characteristics of the $n = 2$ HFAC in JET pulse #95691

	Sawtooth cycle $t = 9.34$-10.23 s		Sawtooth cycle $t = 10.23$-11.74 s	
Time	9.7 s	10.2 s	10.6 s	11.6 s
Frequency	423 kHz	383 kHz	424 kHz	354 kHz
$q_{\min}$	0.89	0.83	0.89	0.80
$\lambda = \omega R_0 / v_{A0}$	0.88	0.79	0.88	0.75

3.3. Assessment of energetic particle drive for HFAC and numerical calculation of the resonance maps.

In order to assess the wave-particle resonant interaction for HFAC, we employ a particle following code HALO [26] which computes full orbits of test energetic particles in toroidal geometry. We find that only those energetic deuterons interact with the modes which are close to the resonance condition

$$\omega - n\omega_\phi(E; P_\phi; \mu) - p\omega_\theta(E; P_\phi; \mu) = 0\,. \qquad (4)$$

Here ω is the mode frequency; n is the toroidal mode number; $\omega_\phi(E; P_\phi; \mu)$ and $\omega_\theta(E; P_\phi; \mu)$ are the toroidal and poloidal frequencies of the unperturbed energetic ion guiding center motion; $E; P_\phi$ and μ are the ion energy, toroidal angular momentum, and magnetic moment, respectively; and p is an integer. Equation (4) selects a thin surface in a three-dimensional space of the energetic ion constants of motion $(E; P_\phi; \mu)$. A single resonance typically involves a relatively small area of phase space within a broader distribution of fast particles. For the case of the $n = 2$ HFAC with $f = 410$ kHz, we find that condition (4) is satisfied for the areas shown in Figure 11(a).

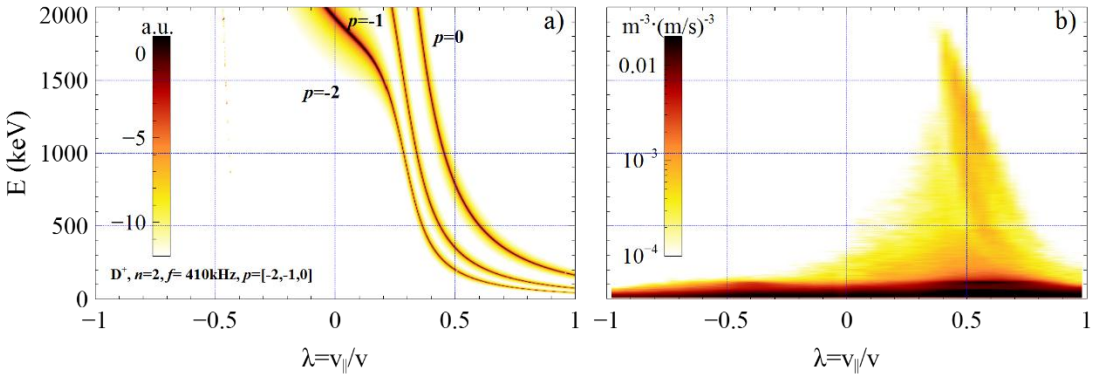

Figure 11. a) The HALO calculation of the regions in energetic ion phase space where the resonance condition (3) is satisfied for the n=2 HFAC mode with frequency 410 kHz. The strongest resonances with integer values of p=0, -1, -2 are shown. b) The distribution function of ICRF-accelerated deuterons at the mode location computed with the TRANSP-TORIC code.

Figure 11(a) shows that the HFAC resonant interaction (and destabilization) could be caused by the passing ions with the pitch-angle close to unity at a rather high energy of several hundred keV. This is in agreement with the JT-60U experimental results [9] which concluded that super-Alfvénic passing ions are necessary to satisfy the resonance condition for HFAC. The resonances (especially the strongest p=0) are found to be well within the computed distribution function of energetic deuterons shown in Figure 11(b). The distribution function is calculated for the D-(D_{NBI})-^{3}He ICRH discharge at the radial location of the HFAC mode with the TRANSP-TORIC code [5].

As HFACs resonate with high-energy passing ions, this explains why HFACs are not often seen in JET experiments (in contrast, the low-frequency ACs can be destabilized by lower energy fast ions, both trapped and passing). Indeed, the commonly used ICRF schemes such as H or ^{3}He minority could generate fast ions in the MeV energy range, but the trapped ones. NBI is commonly the main source of passing fast ions on JET, yet with energies limited to ~125 keV only. The novel three-ion scenarios at JET have a unique feature of generating a large population of passing fast ions of energy ~0.5 MeV and higher [2, 3], thereby mimicking the conditions of earlier JT-60U experiments with negative-ion-based NBI [9]. The observed HFACs could also be highly relevant for future ITER and fusion reactor plasmas dominated by fusion-born alpha-particles, including a large population of MeV-range passing fast ions.

4. Summary and conclusions.

Various types of Alfvén eigenmodes have been observed over a broad frequency range from 80 kHz to 700 kHz in mixed D-^{3}He plasmas heated by the three-ion radio frequency scenario on JET. Radial localization of these AEs was identified with a range of internal diagnostics such as the X-mode reflectometer, multiline interferometer and soft X-ray. An example of the measurements is given for one of the JET discharges, pulse #95691. According to these experimental measurements Alfvén cascades at frequency 80-180 kHz and high frequency Alfvén cascades at 330-450 kHz were localized in the plasma core at $s \approx 0.2$-0.4. The frequency of the high-frequency Alfvén cascades exceeds the frequency of the toroidal Alfvén eigenmodes in contrast to the frequency of usual Alfvén cascades. The AE mode structures calculated with the MHD suite of codes, which includes HELENA, CSCAS and MISHKA, are found to be consistent with the measurements. Eigenmodes of high frequency Alfvén cascades are calculated numerically. These calculations show qualitative agreement with analytical model of high frequency Alfvén cascades [8]. The high frequency Alfvén cascades exist due to the extremum in Alfvén continuum structure caused by the minimum of the safety factor q_{min}, similarly to the low frequency Alfvén cascades. The frequency of the high frequency Alfvén cascades decreases with q_{min} decreasing in contrast to usual Alfvén cascades. Our analysis shows that the HFAC resonant interaction is mostly caused by passing ions at energy of several hundred keV, which are uniquely generated at JET using the three-ion ICRF scheme. The observations of HFACs at JET are consistent with earlier JT-60U experimental results, which concluded that super-Alfvénic passing ions are necessary to satisfy the resonance condition for HFACs [9]. Although HFACs are not often seen on JET, these modes could be highly relevant for future ITER and fusion reactor plasmas dominated by ~MeV energetic ions, including a significant population of passing fast ions that could naturally satisfy the resonant condition found for HFACs.

Acknowledgments.

Important discussions and assistance are greatly appreciated with A. Bierwage, P. Lauber, H.J.C. Oliver, L. Giacomelli. This work has been carried out within the framework of the EUROfusion

Consortium and has received funding from the Euratom research and training programme 2014–2018 and 2019–2020 under Grant Agreement No. 633053. The views and opinions expressed herein do not necessarily reflect those of the European Commission.

References

[1] Kazakov Ye.O. *et al* 2020 *Nucl. Fusion* **60** 112013

[2] Nocente M. *et al* 2020 *Nucl. Fusion* **60** 124006

[3] Kazakov Ye.O. *et al* 2021 *Phys. Plasmas* **28** 020501

[4] Kiptily V.G. *et al* 2021 *Nucl. Fusion* **61** 114006

[5] Štancar Ž. *et al* 2021 *Nucl. Fusion* **61** 126030

[6] Sharapov S.E. *et al* 2002 *Phys. Plasmas* **9** 2027

[7] Nazikian R. *et al* 1997 *Phys. Rev. Lett.* **78** 2976

[8] Breizman B.N. *et al* 2003 *Phys. Plasmas* **10** 3649

[9] Takechi M. *et al* 2005 *Phys. Plasmas* **12** 082509

[10] Huysmans G.T.A. *et al* 1991 *International Journal of Modern Physics C* **02(01)** 371

[11] Kerner W. *et al* 1998 *J. Comput. Phys.* **142** 271

[12] Mikhailovskii A.B. *et al* 1997 *Plasma Phys. Rep*. **23** 841

[13] Breizman B. N. *et al* 2005 *Phys. Plasmas* **12** 112506

[14] Van Zeeland M.A. *et al* 2016 *Nucl. Fusion* **56** 112007

[15] Hacquin S. *et al* 2007 *Plasma Phys. Control. Fusion* **49** 1371

[16] Meneses L. *et al* 2011 *Fusion Eng. Design* **86** 552

[17] Lao L.L. *et al* 1985 *Nucl. Fusion* **25** 1611

[18] Hawkes N.C. and Brix M. 2006 *Review of Scientific Instruments* **77** 10E509

[19] Sirinelli A. *et al* 2010 *Review of Scientific Instruments* **81** 10D939

[20] Salzmann H. *et al* 1988 *Rev. Sci. Instrum.* **59** 1451

[21] Maslov M. *et al* 2013 *JINST* **8** C11009

[22] Nabais F. *et al* 2012 *Nucl. Fusion* **52** 083021

[23] Sharapov S.E. *et al* 2018 *Nucl. Fusion* **58** 082008

[24] Kramer G.J. *et al* 2001 *Nucl. Fusion* **41** 1135

[25] Sharapov S.E. *et al* 2004 *Phys. Plasmas* **11** 2286

[26] Fitzgerald M. *et al* 2020 *Comp. Physics Comm.* **252** 106773